A Robust Approach to Unsupervised Segmentation of Seismic Data Sets

Klaus Köster and Michael Spann
School of Electronic and Electrical Engineering
The University of Birmingham
Pritchatts Road 52, Edgbaston, Birmingham B15 2TT,UK
e-mail: koesterk@eee.bham.ac.uk, M.Spann@bham.ac.uk

Abstract

This paper describes an unsupervised method to extract 2D and 3D inner earth structures from seismic reflection measurements. The application is a typical texture segmentation problem, which can be split up into a feature extraction stage and a segmentation stage. As a texture feature, the locally emergent frequency is estimated by a Gabor filter bank. The instantaneous frequency (IF) has already been succesfully used for seismic trace analysis [12] and will be compared with the results of the filter bank. A second stage of the algorithm involves a region growing method to compute the final object structure. The extremely flexible segmentation scheme is appropriate for application to 2D and 3D data sets of scalar and vectorial data of arbitrary dimensions. The merging decision is based on the mutual inlier ratio at the boundary of two adjacent regions. This ratio is computed by robust regression techniques [11] to avoid noise artifacts. A mutual inlier ratio discrimination function to recognize identical Gaussian distributions guaranteeing a 97.5% certainty is derived. This method is compared with the Kolmogorow-Smirnov-test and results of the application in a segmentation algorithm are shown. The segmentation stage is also tested with different data sets from other computer vision problems to call attention to its general flexibility.

1 Introduction

This work describes an unsupervised method to extract 2D and 3D inner earth structures from seismic reflection measurements in oder to support expert interpretation of the data. The data sets are acquired by a seismic reflection method, which maps the structure of subsurface formations by measuring the times required for a seismic wave to return to the surface. The waves are reflected by interfaces between formations having different physical properties. The reflections are measured by an array of ground motion responsive instruments. A successive migration process converts the measured data into 2D or 3D data sets. By interpreting this data a geophysicist is able to recognise structural features from characteristic variations of the reflection times. The aim of this work is to support the time consuming interpretation process (esp. for 3D data) and to improve its results.

Direct approaches to this problem in the published literature are rare. Ng[10] proposed a supervised method for 2D data. This approach used 3×3 sized bandpass filters to extract characteristic features for a trained segmentation algorithm. The necessary training step limits the number of distinguishable regions and becomes very complex for 3D data.

From a computer vision point of view the task is a general texture segmentation problem, which first extracts characteristic patterns for seismic events (feature extraction stage) and then in a segmentation stage groups data elements with similar patterns to geologic structures (segmentation stage). Taner *et al*[12] discussed a local frequency estimate as a useful feature to describe seismic events. There are several approaches to extract this quantity in the literature [3, 8, 5]. In this work, Gabor filters are applied as they offer the best possible response localisation in the time and frequency domains[4]. Particularly useful tools for geologic interpretation of seismic traces are complex seismic trace analysis [12] and the extraction of the instantaneous frequency (IF). The theory of IF and a discussion of its interpretation can be found in [2]. An important advantage of this quantity is, especially for large 3D data sets, its simple in-place computation. The feature extraction will be elucidated in Section 2. Results of both estimators are compared in Section 4.

The segmentation stage of this work uses a region growing technique based on statistical decision rules. This general technique segments the entire image into

small cells (say 2x2, 4x4 or 8x8 pixels) and merges them based on a statistical measure. A problem of the approach is the lack of data in the beginning, due to the small initial cell size, which imposes a high uncertainty on statistical results. Also a regular grid of initial cells is likely to contain cells lying on the boundary of two or more regions, which makes them difficult to handle in the later merging stage. Rousseeuw [11] proposed the least median of squares (LMedS) estimation technique, which results in robust estimates even when the data set contains up to 50% of outliers. Introducing this technique into computer vision, Meer [9] observed more robust results for smaller sets compared to traditional least squares methods. By using the LMedS properties, together with a shifting technique for overlapping cells, the problem of cells placed on multiple regions is solved in this work. After this tessellation step the algorithm starts with initial cells containing a minimum of outliers and a maximum certainty for the estimated distribution.

The merging stage compares in general the distributions of the initial regions using a hypothesis test and merges them according to the result. An established method for testing is the Kolmogorov-Smirnov test which does not restrict the underlying distribution but is known to be unreliable for small data sets and computationally expensive for larger sets. Meer [9] uses a mutual inlier ratio, which in his work must be larger than a specified fixed value to allow two regions to be merged. Smaller sets imply larger associated statistical uncertainties. Therefore the Meer specified value must be a function of the set size, to ensure that the probability of merging two regions is invariant of the set size. Section 3 describes this idea and the consequences for the segmentation technique. Finally Section 4 displays results for seismic data and for some other 2D and 3D applications of the algorithm. Conclusions are given in Section 5.

2 Feature Extraction

This section describes the feature extraction stage. Two methods for estimating the local frequency in seismic data will be described. Section 2.1 describes an approach using a Gabor filter bank and Section 2.2 elucidates the estimation of instantaneous frequency, a tool applied for seismic data interpretation proposed by Taner[12].

2.1 Gabor Filter Banks

Gabor filters are widely used for extraction of local frequency[3, 4]. A real 2D-Gabor filter averaging in the z direction, can mathematically be described as

$$m(x,y,z) = e^{-\frac{1}{2}\left[\frac{x^2}{\sigma^2}+\frac{y^2}{\sigma^2}+\frac{z^2}{\sigma_z^2}\right]} \cdot \cos\Big(2\pi\mu_0(x\cos\theta + y\sin\theta)\Big), \tag{1}$$

where μ_0 denotes the radial centre frequency and θ the orientation of the Gabor wavelet. As Gabor filters are not separable in the spatial domain, they are computationally very expensive if implemented as convolution masks in the spatial domain. Equation 1 uses the third dimension for smoothing, but assumes that frequency components in this direction are negligible against the contributions in the x- and y-directions. This assumption is valid in the presented data sets, where changes in the z-direction happen to be very smooth. The advantage is the separability of the convolution mask in the z-direction.

To estimate local frequencies, multiple Gabor filters tuned to different frequencies and orientations have to be applied on the data. The filter bank has to cover the frequency bands of the expected signal. The arrangement of filters for this work is derived from [4]. For the application in seismic data, a filter bank of 10×10 filters has been designed with frequencies μ_0 between 0 and π and orientations θ between 0 and 180 degrees in the Fourier domain. The values for μ_0 are $\{0.03, 0.057, 0.086, 0.11, 0.14, 0.169, 0.196, 0.22, 0.25, 0.28\}$ and for the orientations θ $\{0°, 18°, 36°, 54°, 72°, 90°, 108°, 126°, 144°, 162°\}$. To estimate the local emergent frequency the three largest filter responses are stored. If $m_1(\vec{x})$, $m_2(\vec{x})$ and $m_3(\vec{x})$ are the responses of these three filters, $\mu_1(\vec{x})$, $\mu_2(\vec{x})$ and $\mu_3(\vec{x})$ and $\theta_1(\vec{x})$, $\theta_2(\vec{x})$ and $\theta_3(\vec{x})$ are the corresponding centre frequencies and orientations, then the local emergent frequency $\omega(\vec{x})$ and orientation $\Theta(\vec{x})$ are estimated by:

$$\omega(\vec{x}) = \frac{m_2(\vec{x})\mu_1(\vec{x}) + m_2(\vec{x})\mu_2(\vec{x}) + m_2(\vec{x})\mu_3(\vec{x})}{m_1(\vec{x}) + m_2(\vec{x}) + m_3(\vec{x})} \tag{2}$$

$$\Theta(\vec{x}) = \frac{m_1(\vec{x})\theta_1(\vec{x}) + m_2(\vec{x})\theta_2(\vec{x}) + m_3(\vec{x})\theta_3(\vec{x})}{m_1(\vec{x}) + m_2(\vec{x}) + m_3(\vec{x})}. \tag{3}$$

2.2 Instantaneous Frequency Estimation

The model of the real seismic signal is assumed to be of the form

$$s(t) = A(t)\cos\phi(t), \tag{4}$$

where the amplitude $A(t)$ varies slowly with respect to $\cos\phi(t)$. Gabor[6] proposed a method to generate a

unique complex signal, via a Hilbert transform, generally referred to as the analytic signal:

$$\begin{aligned} z(t) &= s(t) + jH[s(t)] \\ &= A(t)(\cos\phi(t) - j\sin\phi(t)) \\ &= A(t)e^{-j\phi(t)}, \end{aligned} \quad (5)$$

where $H[]$ denotes the Hilbert transform. To allow this computation

$$H[s(t)] = H[A(t)\cos\phi(t)] = A(t)H[\cos\phi(t)] \quad (6)$$

has to be valid. The necessary constraint of a slowly varying amplitude has been expressed more specifically by Bedrosian's product theorem for Hilbert transforms[1]. Having computed the analytic signal, the IF $f_i(t)$ can be extracted via:

$$f_i(t) = \frac{1}{2\pi}\frac{d}{dt}\phi(t). \quad (7)$$

The assumed signal model in equation 4 is a generally accepted model for locally narrow-band signals[4]. The computation of the IF does not return meaningful results if this narrow band constraint and Bedrosian's theorem are broken[1, 2]. To get an idea of the signal's local bandwidth, the instantaneous bandwidth (IB) for discrete times can be computed via[5]:

$$b_i(t) = \frac{|z(t)|^2 - |z(t+1)z^*(t-1)|}{|z(t)|^2 + |z(t+1)z^*(t-1)|}, \quad (8)$$

where $z^*(t)$ denotes the conjugate complex value of the analytic signal $z(t)$. $b_i(t)$ has a range of values between 0 and 1. In Taner's paper[12] the results of the IF computation of seismic data contain sharp peaks. Taner uses a weighted average of the IF to emphasise the IF of stronger reflection events and to smooth noise artifacts. Figure 1 illustrates a real seismic signal with computed IF and IB. The peaks in the IF estimate always occur with a peak in the IB showing that the narrow band constraint is violated and the IF estimate is erroneous at this time.

The IF value is the time derivative of the instantaneous phase $\phi(t)$. By taking the x- and y-axis (and z-axis for 3D data) of the input set as the time axis two (three) values are computed per pixel (voxel). The final feature is therefore a vector.

3 The Segmentation Algorithm

The region-growing algorithm works in a bottom-up way generating an irregular graph pyramid to store neighbourhood relations between regions. Each graph node represents a region in the image and contains the parameters of a data model described in Section 3.1. The initial cell tessellation is the lower of two hierarchies and its generation will be described in Section 3.2. Starting from this level, higher hierarchies of primitive regions (PR) are computed by merging the cells in the level below. The merging decision is described in Section 3.3. Based on this decision rule Section 3.4 describes the generation of the first PR hierarchy and Section 3.5 elucidates an iterative merging strategy leading to the final 2D or 3D region map.

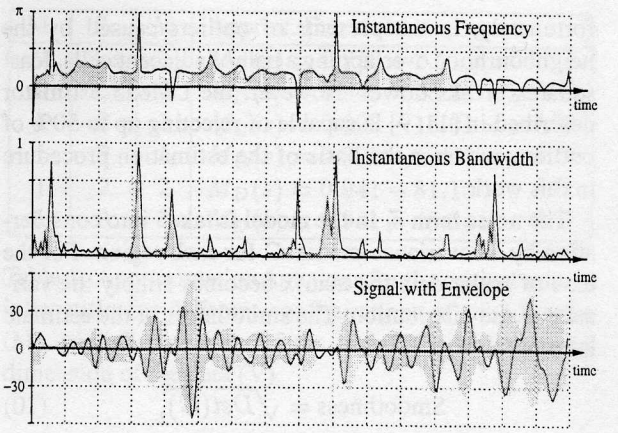

Figure 1: Seismic signal over time with envelope, instantaneous bandwidth (IB) and instantaneous frequency (IF) displays a strong correlation of peaks in the IF with high IB values.

One of the design goals of the algorithm was to keep its mathematics and methods as free as possible from constraints imposed by the spatial dimension of the input image or the data dimension (scalar or vectorial data). This allows an application of the same technique to a range of completely different segmentation problems and might give the reader a better idea of the flexibility of this technique.

3.1 The Data Model

A polynomial description of the region data has been chosen. The implementation supports zero- and first-order models for 2D and 3D images of scalar or arbitrary dimensional, vectorial data. As space is limited only the model for 3D images, first order models and vectorial input data will be described. Other configurations can easily be derived from these results.

Given a set of voxels $V = \{\vec{v}_1, \vec{v}_2, \ldots\}$, the data model is specified by

$$\vec{v}_i(x,y,z) = \vec{a}_x x + \vec{a}_y y + \vec{a}_z z + \vec{a}_0 + \vec{e}_i, \quad (9)$$

where the $\vec{a}_{\{x,y,z,0\}}$ denote the model parameters and $\vec{e}_i$ is an independent additive normally distributed noise term. For this case the model parameters can be estimated by minimum least squares (LS) techniques. Un-

fortunately, in the presents of outliers caused by the neighbourhood overlapping a pair of adjacent cells, least squares breaks down. However, the LMedS estimator described in [11, 9] is capable of rejecting up to 50% of outliers, which is the basis of the estimation procedure in this work.

The noise term $\vec{e}_i$ in the model is taken into consideration by a covariance matrix $\boldsymbol{C}$ for each region. For the case of scalar data the matrix becomes simply the variance of the distribution. The smoothness of the estimate is computed by:

$$\text{Smoothness} = \sqrt{Det(\boldsymbol{C})}, \tag{10}$$

where $Det()$ denotes the determinant. Since a covariance matrix can be seen as a general description of an ellipsoid, the smoothness value can also be interpreted as the volume of the ellipsoid[11].

To test whether a sample p is an inlier within the model, the decision rule[1],

$$\left(\vec{p} - \hat{\vec{v}}_i\right)\boldsymbol{C}^{-1}\left(\vec{p} - \hat{\vec{v}}_i\right)^T \leq \chi^2_{p,0.975} \tag{11}$$

has to be true. $\hat{\vec{v}}$ denotes the LMedS computed estimation. The value $\chi^2_{p,0.975}$ is from chi-square statistics and p denotes the degrees of freedom, which is equal to the vectorial dimension of the data in this case. The left part of the relation expresses also a relative distance of the point $\vec{p}(x, y, z)$ from the data model. Expression 11 is true for 97.5% of the samples of a p-dimensional Gaussian distribution. The advantage of this decision rule and the above defined measure of smoothness is that both are applicable for arbitrary polynomial degrees and vectorial dimensions.

3.2 Initial Segmentation Stage

The original data set is tessellated with cells of $3 \times 3 \times 3$ voxels for the 3D case and 5×5 pixels for segmentation of 2D images. The initial size is a trade-off between statistical robustness, which requires larger sets when estimating model parameters, and good precision for detecting small regions, which needs small basic elements for later merging. The LMedS estimator is applied for each cell to estimate the model parameters. The cells are overlapping by 2 voxels (4 pixels in 2D) in each dimension. A regular tessellation is likely to contain cells placed on a boundary of two or more regions. To avoid this the initial cells are shifted. The smoothness criterion described in equation 10 will return large values for cells placed on a boundary. Therefore each cell is shifted by at most one voxel (2 pixels in 2D) per direction to a position resulting in a local minimum of the smoothness criterion. Figure 2 illustrates this step. The initial cells are overlapping to avoid any voxels (pixels in 2D) not being covered by any cell after the shifting procedure. This cannot be avoided for a few pixels at the image boundary. By shifting the cells the initial tessellation can be adapted to almost any region structure and the final segmentation will not contain the "block-structure" of the initial cells.

[1] The coordinates have been dropped for convenience.

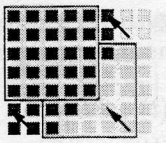

Figure 2: Shifting of the initial cells. The cells, marked by a frame, are shifted to a position resulting in a local minimum of the robust smoothness criterion to avoid cells placed on region boundaries.

3.3 Region Merging based on the Mutual Inlier Ratio

In general the merging stage of a region-growing algorithm compares statistical measures of two adjacent regions and merges them or not according to the test result. This algorithm uses the mutual inlier ratio to come to a decision assuming a Gaussian distribution for the elements of a set. Let R_A be the set of elements of region A. The set of inliers I_A of region A is

$$I_A = \left\{\vec{v} \in R_A : (\vec{v} - \vec{v}_A)\boldsymbol{C}_A^{-1}(\vec{v} - \vec{v}_A)^T \leq \chi^2_{p,0.975}\right\}, \tag{12}$$

where $\vec{v}_A$ denotes the result of the model of Region A and $\boldsymbol{C}_A^{-1}$ is the inverse of its covariance matrix. The coordinates of the vectors have been dropped for convenience. To determine the mutual inlier ratio M_{AB} of two regions A and B, the inliers of A which are also inlying in B have to be determined:

$$I_{AB} = \left\{\vec{v} \in I_A : (\vec{v} - \vec{v}_B)\boldsymbol{C}_B^{-1}(\vec{v} - \vec{v}_B)^T \leq \chi^2_{p,0.975}\right\}. \tag{13}$$

Now the mutual inlier ratio M_{AB} becomes:

$$M_{AB} = \frac{\mathfrak{card}(I_{AB})}{\mathfrak{card}(I_A)}, \tag{14}$$

where the operator $\mathfrak{card}()$ returns the number of elements of a set.

Having computed the ratio, one has to compare the result with a discriminating value. If the ratio is larger than this value, then the two distributions are found to be

similar. A safe test result can only be obtained if the similarly computed M_{BA} is also larger than the discriminating value. This avoids the situation where regions with large variances accept too many adjacent regions with smaller variances as inliers leading to an over-merged result. Certainly the discriminating value is a crucial value and determines the size of merged regions significantly. In the sequel an expression for the discriminating value will be determined.

It is a well-known fact that the quality of a statistical estimate of a data set's distribution parameters depends on the size of the set. High levels of both precision and reliability can be achieved by increasing the sample size. For a region merging algorithm, where the initial region size is in general limited, the exact estimation of the model parameters suffers from the standard deviation of the model σ and from an additional finite sample size error, which decreases with growing set size n. The relationship between the exact unknown mean of a distribution μ and the estimated mean $\bar{X}$ can be expressed by[7]:

$$\mu = \bar{X} \pm d, \qquad d = t_{0.975}\frac{s}{\sqrt{n}}, \tag{15}$$

where s denotes the estimated standard deviation, n is the set size and $t_{0.975}$ is based on the Student t distribution with a 97.5% confidence interval allowing us to use the estimated standard deviation instead of the true (unknown) standard deviation. Having two estimates of the same distribution, the worst case occurs if estimate $\bar{X}_1$ equals $\mu + d_1$ and estimate $\bar{X}_2$ is computed as $\mu - d_2$. A discrimination value M_{DISC} finding the two estimates of the same distribution to be similar in this worst case can theoretically be determined by solving the integral over the overlapping inlier area of the two estimated distributions:

$$M_{\text{DISC}} = \frac{1}{\sqrt{2\pi}s_1} \int_{\bar{X}_1 - s_1\sqrt{\chi^2_{p,0.975}}}^{\bar{X}_2 + s_2\sqrt{\chi^2_{p,0.975}}} e^{-\frac{(x-\bar{X}_1)^2}{2s_1^2}} dx \tag{16}$$

According to the chosen χ^2-value $M_{\text{DISC},97.5\%}$ should be 0.975 for a set of infinite size as the finite set error d disappears. It is difficult to find a closed expression for this error approximation, since it still contains the estimated standard deviations s_1 and s_2. Nevertheless the discrimination value $M_{\text{DISC},97.5\%}$ can be measured for different configurations of model degree, spatial dimension of the image and data dimension. Here two sets of Gaussian distributed independent vectors are generated, their distribution is estimated and the two mutual inlier ratios are stored. This experiment is repeated 400 times to get a reasonable certainty. From the stored inlier ratios the $(1.0 - 0.975) \times 2 \times 400$th smallest one is picked as the discrimination value for the current configuration. This measurement has been repeated for set sizes between 20 and 1000. The result is discrimination values for the inlier ratio which allow recognition of identical Gaussian distributed sets with a certainty of 97.5%. It is important to note that these results have been measured with the LMedS estimator. This estimator is not optimal for Gaussian noise, as are for example LS-methods[9], but as this estimator is used in the algorithm it is reasonable to use it in the measurement of this discrimination function as well.

M.	S.	V.	Approx. Func.
0	2,3	1	$M_D(s) = 0.953 - 2.11 \times s^{-0.78}$
0	2,3	2	$M_D(s) = 0.943 - 26.31 \times s^{-1.37}$
1	2	1	$M_D(s) = 0.923 - 16.01 \times s^{-1.08}$
1	3	1	$M_D(s) = 0.928 - 19.96 \times s^{-1.1}$
1	2	2	$M_D(s) = 0.941 - 81.19 \times s^{-1.59}$
1	3	2	$M_D(s) = 0.941 - 48.34 \times s^{-1.46}$

Table 1: Approximation functions for the critical mutual inlier ratio for different configurations of model order (M), spatial dimension of the image (S) and vectorial dimension of the data (V).

The measured values have been approximated by a function to avoid storing them explicitly. The utilised approximation function is of the form $M_{\text{DISC},97.5\%}(size) = a - b \times size^{-c}$. Table 1 displays approximating functions for some configurations. The parameters a, b and c are computed by least squares regression of the measured values. Figure 3(a) displays the measured values and the approximating function for the case of a zero order polynomial model in a 2D image with scalar data.

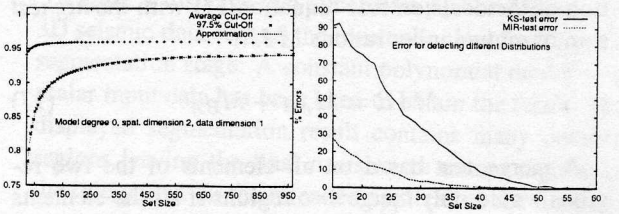

(a) (b)

Figure 3: Average discrimination value, 97.5% discrimination value and approximation (a). Comparison of mutual inlier ratio with KS-test (b). The discrimination error of both methods for two significantly different distributions is measured.

To compare the mutual inlier ratio with an established method two Gaussian distributed sets of significantly different mean and variance were created and examined by the KS-test and the mutual inlier test. Figure 3(b) dis-

plays the error rates for 2000 tests using sets with sizes between 15 and 60. It should be kept in mind that the KS-test does not assume any distribution, while the inlier ratio assumes Gaussian statistics to detect outliers. The figure shows a significantly greater reliability when using the mutual inlier ratio for small sets, which is a crucial property for a region-growing algorithm.

3.4 Primitive Region Generation Stage

This stage of the algorithm generates a first PR hierarchy by merging the initial cells. The stage starts by sorting the cells according to their smoothness ("volume"). A first PR is created and the smallest-volume-cell is added to this region. Next all spatially adjacent neighbours of this cell are visited recursively, becoming a member of the PR if they are inliers within the model of all of the other cells of the PR. The recursion stops if an adjacent cell does not satisfy the merging rule. The inlier decision is found by the described mutual inlier ratio. If no further adjacent cells can be added to the first PR, a new PR is started with the next available smallest-volume cell. Again the neighbours of this cell are visited recursively. This step is repeated until every cell is associated with a PR. The sorting step in the beginning of this stage avoids over-merging since cells with a large variance tend to accept other cells more easily as inliers because of the "large volume"- covariance matrix.

3.5 Iterative Region Merging Stage

This final stage of the algorithm iteratively merges the PRs until no adjacent region pair satisfies the merging rule. Each iterative merging step starts by constructing a link to the neighbour, which results in a mutual satisfaction of the decision rule (equation 11) with the *highest* sum of mutual inlier rations MIR:

$$MIR = M_{AB} + M_{BA}. \qquad (17)$$

A merge test based on all elements of the two regions would only merge two regions if all the elements strictly belong to the estimated model. By using only data close to the boundary of the two examined regions (local data), smooth model changes within a region are also tolerated. The local data consists of elements of cells placed at the boundary of the two PRs. The boundary cells are recognised in the graph hierarchy since they possess a neighbouring cell whose parent is the other PR considered in the merge test. In figure 4(a) these boundary cells are marked by a darker background.

The stage starts merging the PRs after the best neighbour for merging has been determined for each PR. Each PR satisfying the merge test with one of its neighbours,

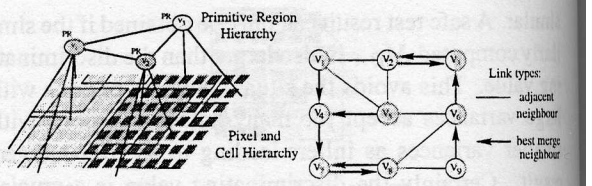

(a) (b)

Figure 4: Data hierarchy of the algorithm (a). Displayed are the initial cells with parent links to the PRs. Each PR contains a set spatially adjacent neighbours links. The pixels of the two regions are symbolised by squares with different greylevel. Figure (b) displays the regions ν_i having a link to their neighbour being most qualified for merging.

is linked to that neighbour, which results in the maximum MIR. However neighbouring PR's are *not* necessarily mutually optimal, e.g. in figure 4(b) PR ν_6 optimises the MIR for PR ν_9 even though ν_9 does not optimise the MIR for ν_6. The links build up "chains" ending in a mutually best-neighbour pair. Only these pairs are merged in each iteration to avoid over-merging. Others might be connected in later iterative steps if the merging criteria are still satisfied. In figure 4(b) only regions ν_2 and ν_3 and regions ν_7 and ν_8 would qualify for merging according to this rule.

This iterative merging strategy has the advantage of being independent of the order of visiting the PRs. Therefore the iterative step can be implemented in parallel using multiprocessor architectures.

4 Experimental Results

This section shows some results of the feature extraction stage and the segmentation. The two local frequency estimators are tested on synthetic and real seismic images provided by the project sponsor. It is very difficult in general (and also subjective) to find ground truth for real seismic images. Therefore the segmentation stage is firstly tested on a 3D MRI measurement and an a range image, to point out some of its properties. Finally some segmentation results for real seismic data will be shown.

4.1 Feature Extraction in Seismic Data

Figure 5(a) displays a 2D synthetic data set and the results obtained from the IF estimation (b) and the bank of Gabor filters (d). A higher greylevel codes a higher estimated local frequency. The frequency measurements are, qualitatively, strongly in agreement with the pattern in the top part of the image. Although the Gabor filter responds with small deviations at the pattern boundaries, details in the bottom part of the image are distinguished

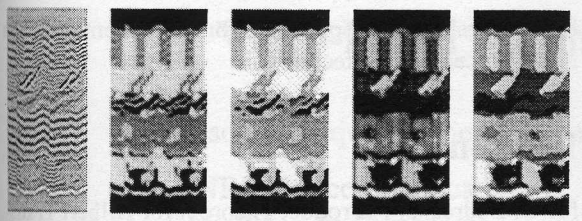

(a) (b) (c) (d) (e)

Figure 5: 2D synthetic seismic image provided by Shell Research, The Netherlands (a) and results obtained from the IF estimator in vertical direction (b) and segmentation (c). Result of bank of 10×10 Gabor filters (d) and segmentation (e).

slightly better than by the IF approach. To compute the IF the data set has to be Fourier transformed, multiplied and inversely Fourier transformed, while each Gabor filter requires a convolution of the whole data set. Therefore the IF offers a significant computational advantage, especially for larger 3D data sets.

A major problem of the IF estimation in seismic data are the described peaks in the estimates due to the violation of the narrow band constraint of the assumed model (equation 4). Although the Gabor filter approach assumes a similar model[4], the results do not contain these artifacts and provide especially for real data a more robust base for the unsupervised segmentation stage.

4.2 Segmentation Algorithm

To test the segmentation precision of the algorithm, a data set containing 3D range measurement was segmented. Figure 6 displays the range image[2], and the obtained region map. For the range image segmentation we have used a first order polynomial model. Using a final boundary refinement based on the model and the outlier discrimination rule (expression 11) we obtain the result displayed in figure 6(b). The boundaries have been detected with a very good precision. We found it difficult to detect long thin regions (< 3 pixels) due to the PC mask size. However, these regions can be detected as outliers within the resulting regions. Such a step was not necessary for seismic data.

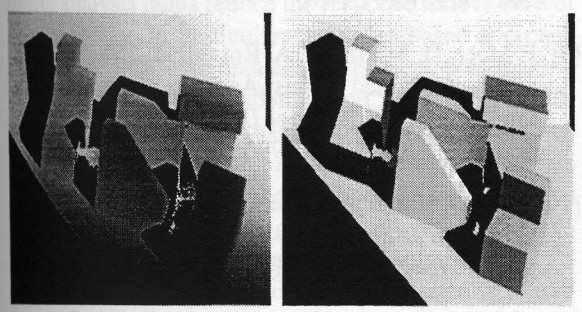

(a) (b)

Figure 6: Segmentation result of range data. Figure (a) shows the range image and (b) displays the segmentation result.

[2]Available from *http://marathon.csee.usf.edu/range/seg-comp/SegComp.html*

Figure 7(a-c) shows three slices of a 3D MRI data set and the corresponding segmented slices. The result was obtained using a constant data model. The example contains some long thin regions, which have been merged to adjacent regions in the result. To be detected a region has to cover a least half of an initial cell due to the LMedS estimator. The initial cells will shift away from regions, which are too thin to fulfil this constraint. Nevertheless these regions can be recovered as their voxels (pixels in 2D) are outliers within the adjacent region being merged to. Finally figure 7(d) illustrates a 3D voxel model of the segmented image.

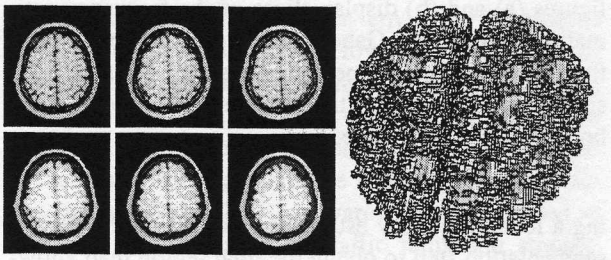

(a) (b) (c) (d)

Figure 7: Slices of 3D MRI data and resulting segmentations (a-c). 3D voxel visualisation of the brain obtained from a 256x256x45 voxel data set.

Figure 8 displays two slices of a Gabor filtered real 3D seismic data set and the result obtained from the 3D segmentation stage. A constant polynomial model with scalar input data has been used to obtain the result. The displayed segmentation result contains many detailed regions leaving the final decision to merge regions to the interpreter. In the intended application the financial consequences of over-merging are possibly much worse than for under-merging. Therefore a greater amount of autonomy is allowed for the human interpreter in this case. The displayed 3D model of the two major structures in the bottom half of the image in figure 8(c) is obtained by manually merging the algorithm's result.

5 Conclusions

This paper has described a system for 2D and 3D processing of seismic reflection data. The system starts by extracting information on geologic structures by apply-

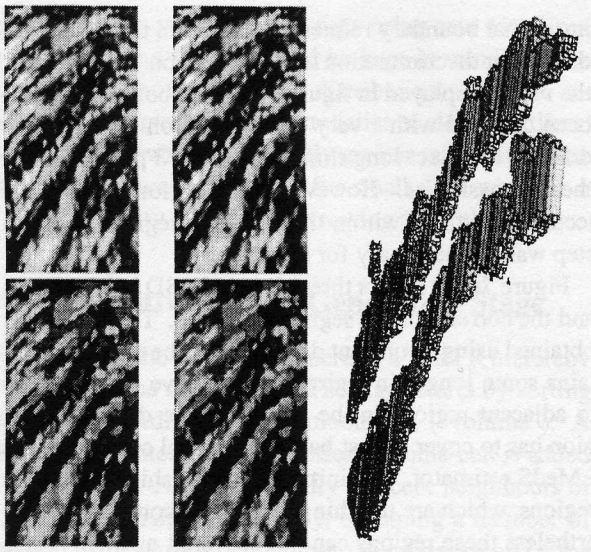

(a) (b) (c)

Figure 8: Segmentation of a real 3D seismic set. Top of figures (a) and (b) display slices of the frequency estimation result of the Gabor bank and the bottom figures the corresponding segmentation results. Figure (c) visualises a 3D model of the two diagonal regions in the bottom part of the image.

ing a local frequency estimator and uses the result in a segmentation step to obtain the final region map allowing a 3D object visualisation.

Two methods to extract geological structure have been examined. A bank of Gabor filters extracts the geological features with good precision but is computationally demanding since Gabor filter masks are not separable spatially. The second method, instantaneous frequency, is easier to compute and has already proven to be a useful tool for interpreting seismic traces. Nevertheless in real seismic data the assumed narrow band constraint of the data model is violated frequently, resulting in sharp "jumps" in the estimate. This effect makes an unsupervised segmentation difficult.

The second stage of the system generates a 2D or 3D structure map based on the extracted feature by applying a robust-region growing technique. A new shift technique for the initial cells using the LMedS estimator enables the initial tessellation to adapt to any 2D or 3D region shape. The algorithm does not need any parameters and is completely free from any assumptions on region number or size. A merging technique has been proposed offering a high robustness especially at the crucial initial merging stage of the algorithm, where statistical estimates possess a high uncertainty due to small set sizes. The technique is not limited to scalar data as it does not involve any sorting etc.. The segmentation stage of the system, as well as the feature extraction, are highly parallel and appropriate for implementations on multi-processor architectures.

References

[1] E. Bedrosian A Product Theorem for Hilbert Transforms. *Proceedings of the IEEE*, 51:868-869, 1963.

[2] B. Boashash. Estimating and Interpreting the Instantaneous Frequency of a Signal - Part 1: Fundamentals. *Proceedings of the IEEE*, 80(4):521 - 538, 1992.

[3] A.C. Bovik. Analysis of Multichannel Narrow-Band Filters for Image Texture Segmentation. *IEEE Transactions on Signal Processing*,39(9),1991.

[4] A.C. Bovik and N. Gopal and T. Emmoth and A. Restrepo. Localised Measurement of Emergent Image Frequencies by Gabor Wavelets. *IEEE Transactions on Information Theory*, 38(2), 1992.

[5] T.A.C.M. Claasen and W.F.G. Mecklenbräuker. The Wigner Distribution - A Tool for Time-Frequency Signal Analysis, Part 1-3. *Philips Journal of Research*, 35(3):217-250, 35(4-5):276-300, 35(6):372-389, 1980.

[6] D. Gabor. Theory of Communication. *Proceedings IEE*, 93(3):429-457, 1946.

[7] L.L. Lapin. Probability and Statistics for Modern Engineering. *2nd ed., PWS-Kent. Boston, MA*, 1990.

[8] S.G. Mallat. A Theory for Multi-Resolution Signal Decomposition: The Wavelet Representation. *IEEE Transactions on Pattern Analysis and Mashine Intelligence*, 11(7), 1990.

[9] P. Meer, D. Mintz and A. Rosenfeld. Least Median of Squares Based Robust Analysis of Image Structure. *Proc. DARPA Image Underst. Workshop*, Pittsburgh, P. A., 231-254, 1990.

[10] I. Ng, J. Kittler and J. Illingworth. Supervised Segmentation using a Multi-Resolution Data Representation. *Signal Processing*, 31: 133-163, 1993.

[11] P.J. Rousseeuw and A.M. Leroy. Robust Regression and Outlier Detection. *Wiley*, New York, 1987.

[12] M.F. Taner, F. Koehler and R.E. Sheriff. Complex Seismic Trace Analysis. *Geophysics*, 44(6): 1041-1063, 1979.